

Spectral Response of Disorder-Free Localized Lattice Gauge Theories

Nilotpal Chakraborty^{1,*}, Markus Heyl^{1,2}, Petr Karpov¹, and Roderich Moessner¹

¹Max-Planck-Institut für Physik komplexer Systeme, Nöthnitzer Straße 38, Dresden 01187, Germany

²Theoretical Physics III, Center for Electronic Correlations and Magnetism, Institute of Physics, University of Augsburg, D-86135 Augsburg, Germany

 (Received 12 January 2023; accepted 31 October 2023; published 29 November 2023)

We show that certain lattice gauge theories exhibiting disorder-free localization have a characteristic response in spatially averaged spectral functions: a few sharp peaks combined with vanishing response in the zero frequency limit. This reflects the discrete spectra of small clusters of kinetically active regions formed in such gauge theories when they fragment into spatially finite clusters in the localized phase due to the presence of static charges. We obtain the transverse component of the dynamic structure factor, which is probed by neutron scattering experiments, deep in this phase from a combination of analytical estimates and a numerical cluster expansion. We also show that local spectral functions of large finite clusters host discrete peaks whose positions agree with our analytical estimates. Further, information spreading, diagnosed by an unequal time commutator, halts due to real space fragmentation. Our results can be used to distinguish the disorder-free localized phase from conventional paramagnetic counterparts in those frustrated magnets which might realize such an emergent gauge theory.

DOI: [10.1103/PhysRevLett.131.220402](https://doi.org/10.1103/PhysRevLett.131.220402)

Lattice gauge theories emerge as low-energy effective theories in a large class of models relevant to quantum many-body physics, especially in frustrated magnets [1,2]. For example, in quantum spin ice and hardcore dimer models, local constraints (such as the ice rule of two spins pointing in and two pointing out locally) yield a $3 + 1$ dimensional compact $U(1)$ lattice gauge theory [3,4]. The resulting algebraic spin correlations are, strictly speaking, only present at zero temperature, in the absence of charges (i.e., violations of the constraints). However, perhaps somewhat counterintuitively, one can also find new phases by creating a high density of such charges, provided that these are static. The concomitant sectors of the lattice gauge theories have been shown to exhibit disorder-free localization in one [5,6] and two dimensions [7,8]. It thus becomes necessary to distinguish disorder-free localization from a paramagnet, the “standard” disordered phase, leading to the twin questions of to what extent one can access novel phases at a finite density of static charges, and above all, what are the distinguishing characteristics of the localized phases?

Here, we present a spectral response dominated by discrete sharp peaks, combined with vanishing weight in

the zero frequency limit, as a characteristic signature of the disorder-free localized phase. We show that such a response arises due to formation of local motifs with discrete spectra in such lattice gauge theories, a feature absent in conventional paramagnets which behave diffusively at high temperatures [9]. We numerically obtain the spectral functions by calculating quantum dynamics of the $2 + 1D$ $U(1)$ quantum link model (QLM) via a controlled cluster expansion method which allows us to access the dynamics deep in the localized phase. Our conclusions are applicable to a large class of lattice gauge theories with discrete degrees of freedom and static charges, of which the $U(1)$ QLM is a prototypical example.

Besides the main result we also show that (i) disorder-free localized lattice gauge theories show information freezing due to real-space fragmentation in 2D. (ii) In different regimes of the $U(1)$ QLM, local and global response of spatially averaged spectral functions differ and such a difference could be measured via local spectroscopy, serving as additional evidence for such physics. There has also been a recent surge in proposals for disorder-free localization [10–13], and stabilizing disorder-free localization on quantum simulators [14]. Hence, distinct experimental signatures are of great current relevance.

Quantum link model and percolation.—The QLM is a discrete version of Wilsonian lattice gauge theories also occurring in gauge magnets [15–18]. Several models in condensed matter, for example, the toric code [19] and quantum dimer and ice models [20–22], can be cast as QLMs. We use the $2 + 1D$ $U(1)$ QLM

Published by the American Physical Society under the terms of the [Creative Commons Attribution 4.0 International](https://creativecommons.org/licenses/by/4.0/) license. Further distribution of this work must maintain attribution to the author(s) and the published article's title, journal citation, and DOI. Open access publication funded by the Max Planck Society.

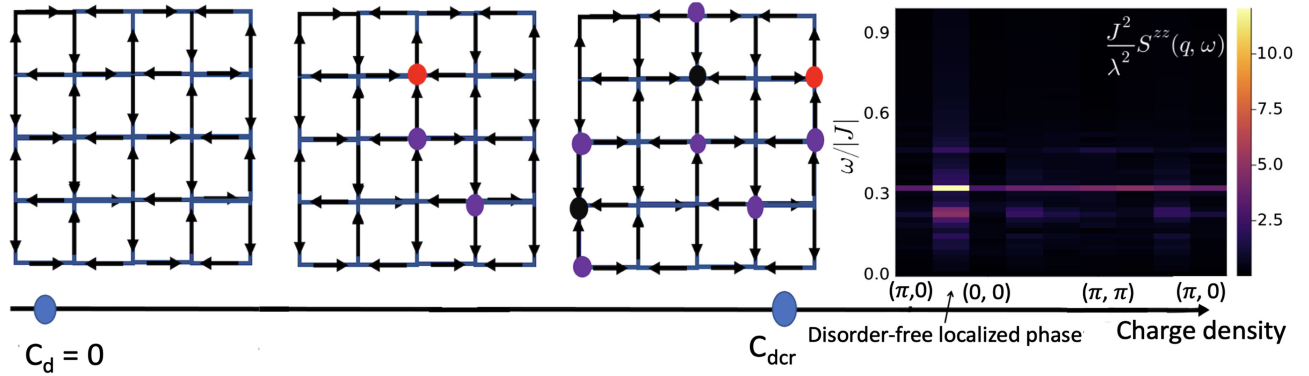


FIG. 1. Accessing novel phases by increasing charge density C_d (colored circles: red, purple, and black for $q_r = -1, 1,$ and -2 , the arrows \rightarrow and \downarrow represent spin $|\uparrow\rangle$, whereas \leftarrow and \uparrow represent $|\downarrow\rangle$). In the presence of a sufficient density of static charges, one can access the disorder-free localized (DFL) phase ($C_d > C_{dcr}$). Rightmost panel: sharp spectral response in spatially averaged spectral functions (in this case, the transverse component of the dynamical structure factor for $|\lambda/J| = 0.2$) with $S^{zz}(q, \omega) \rightarrow 0$ as $\omega \rightarrow 0$, in the disorder-free localized phase.

$$\hat{H} = J \sum_{\square} (\hat{U}_{\square} + \hat{U}_{\square}^{\dagger}) - \lambda \sum_{\square} (\hat{U}_{\square} + \hat{U}_{\square}^{\dagger})^2, \quad (1)$$

where $\hat{U}_{\square} = \hat{S}_{\mathbf{r},\hat{x}}^{+} \hat{S}_{\mathbf{r}+\hat{x},\hat{y}}^{+} \hat{S}_{\mathbf{r}+\hat{y},\hat{x}}^{-} \hat{S}_{\mathbf{r},\hat{y}}^{-}$ flips all spins on a plaquette if they satisfy a certain orientation (clockwise or anticlockwise in Fig. 1). Here, $\hat{S}_{\mathbf{r},\hat{\mu}}^{+/-}$ denotes the spin raising and lowering operators for the spin joining sites \mathbf{r} and $\mathbf{r} + \hat{\mu}$, where $\hat{\mu} = \hat{x}/\hat{y}$ is a lattice vector. The first term in Eq. (1) is a kinetic energy term, whereas the second is a potential energy term [20]. Spin configurations are characterized by the set of static charges on all sites and the charge on each site q_r is determined by the eigenvalue equation of the generator of gauge transformations (which evaluates the difference in incoming and outgoing arrows from a site, see Fig. 1), $G_r|\psi\rangle = q_r|\psi\rangle$ [6] [see Supplemental Material (SM) [23] for expressions of G_r]. The gauge invariance is a statement of charge conservation in this analogy, flipping all spins connected to a site r will not change q_r . For spin-1/2, $q_r \in \{-2, -1, 0, 1, 2\}$. This model has been shown to exhibit disorder-free localization [7,8]. Crucially, the charges are static in our model, and correspond to violations of the ice rule. States belonging to such charged sectors are akin to configurations with defects in frustrated magnets. However, there is no real disorder in the problem, it arises dynamically when considering combinations of sectors with different charge configurations.

We consider the problem with Eq. (1) as the effective Hamiltonian. Without any static background charges we get square ice, i.e., two in and two out spins on every vertex. On increasing the charge density beyond a critical C_{dcr} , there is a disorder-free localized phase [7,8]. If these charges are thermally activated, the disorder-free localized phase would correspond to a high temperature phase (proposed in a different context for 1D [27]). Temperature-dependent dynamics for gauge theories has also been studied in the Kitaev model [28].

Our disorder-free localization can be studied using a percolation model, where one starts from a classical random spin configuration, a random state from the infinite temperature thermal ensemble (drawn from the superposition of all possible sectors, see SM), which fixes the initial charge configuration, and then tracks all possible spin configurations induced by single plaquette flips [first term in Eq. (1)] (see SM for discussion). Plaquette dynamics in such a model is constrained by the static charge environment and certain charge configurations will render a subset of plaquettes permanently frozen. If the initial state hosts a sufficient density of background charges to fragment the lattice into disconnected finite clusters of kinetically active plaquettes, localization ensues (see SM for details on disorder-free localization and percolation).

Effective exact diagonalization using cluster expansion in the localized phase.—We employ an effective exact diagonalization (ED) procedure to calculate the quantum dynamics of our 2D interacting system deep in the localized phase. The percolation model gives us the real-space cluster structure, which in the localized phase comprises only finite disconnected clusters. In contrast, in the delocalized phase there is an infinite percolating cluster coexisting with the finite clusters.

The decomposition of the lattice into only finite clusters in the localized phase due to kinetic constraints, allows us to calculate quantum dynamics for all times using a cluster expansion approach [8]. To calculate spatially averaged expectation values of time-dependent correlation functions for the whole lattice, we start by calculating the quantum dynamics individually for each cluster using exact diagonalization. We then sum the results for all clusters up to a certain size after which we find that including larger clusters adds negligible weight to our observables. Allowed plaquette configurations in a cluster are connected via subsequent single plaquette flips, whereas plaquettes belonging to different clusters (disjoint in real space) are

uncorrelated. Since we calculate dynamical expectation values of two point correlators, the only nonzero contributions come from pairs of spins belonging to the same cluster. Note that our cutoff procedure works well away from the critical regime, in the localized phase, where mean cluster size of the corresponding nonpercolating phase is not too large (see Ref. [23] which includes [24–26]). On approaching the transition, the mean cluster size increases significantly and contributions from finite but large clusters become important and the problem goes beyond our ED.

Frozen spins also contribute a delta function response exactly at zero frequency. However, our results pertain to dynamical spins and since one cannot measure strictly zero frequency, we ignore this contribution and frozen spins are only included in the averaging for calculating global spectral functions. Besides global response, we also calculate local spectral functions, spatially averaged over a finite cluster by averaging over all spins belonging to all clusters of a particular size, obtained from multiple initial random spin configurations.

Information freezing due to fragmentation.—We use our method to first calculate unequal time commutators which are related to the susceptibility via the Kubo formula. Such commutators (also their relatives, the out-of-time-ordered correlators) quantify information spreading, a quantity related to entanglement growth, and have been a measure of chaos and Hilbert-space fragmentation in quantum many-body systems [29–32]. We calculate

$$\begin{aligned}
 C_G(d, t) &= \frac{1}{N} \sum_{\mathbf{r}_i, \mathbf{r}_j \in \mathcal{L}} \langle \psi | [\widehat{S}_{\mathbf{r}_i, \boldsymbol{\mu}}^z(t), \widehat{S}_{\mathbf{r}_j, \boldsymbol{\mu}'}^z(0)] | \psi \rangle \\
 &= \frac{1}{N_d} \sum_{|\text{cl}| < P_c} \sum_{\mathbf{r}_i, \mathbf{r}_j \in \text{cl}} \langle \psi_{\text{cl}} | [\widehat{S}_{\mathbf{r}_i, \boldsymbol{\mu}}^z(t), \widehat{S}_{\mathbf{r}_j, \boldsymbol{\mu}'}^z(0)] | \psi_{\text{cl}} \rangle \\
 C_L(d, t) &= \frac{1}{N'_d} \sum_{|\text{cl}| = P} \sum_{\mathbf{r}_i, \mathbf{r}_j \in \text{cl}} \langle \psi_{\text{cl}} | [\widehat{S}_{\mathbf{r}_i, \boldsymbol{\mu}}^z(t), \widehat{S}_{\mathbf{r}_j, \boldsymbol{\mu}'}^z(0)] | \psi_{\text{cl}} \rangle \quad (2)
 \end{aligned}$$

where $\boldsymbol{\mu} = \hat{x}/\hat{y}$, $A \equiv |\mathbf{r}_i + \boldsymbol{\mu}/2 - \mathbf{r}_j - \boldsymbol{\mu}'/2| = d$, $|\psi_{\text{cl}}\rangle$ is a Haar random state drawn from the Hilbert space spanned by all possible configuration states of the cluster cl and N_d is the number of pairs of spins in the lattice \mathcal{L} separated by distance d , excluding the pairs of spins that belong to all clusters of size $|\text{cl}| > P_c$ as per our method ($P_c = 18$ for this Letter, see SM for details). N'_d is the number of pairs of spins separated by distance d in all clusters with P plaquettes.

We analyze global information spreading represented by $C_G(d, t)$ in Eq. (2), related to entanglement growth in the full system as well as local information spreading $C_L(d, t)$, related to the same in a finite size cluster. Figures 2(a) and 2(b) display a stark difference between the two cases in the $|\lambda/J| \ll 1$ regime. There is a signal up to large distances

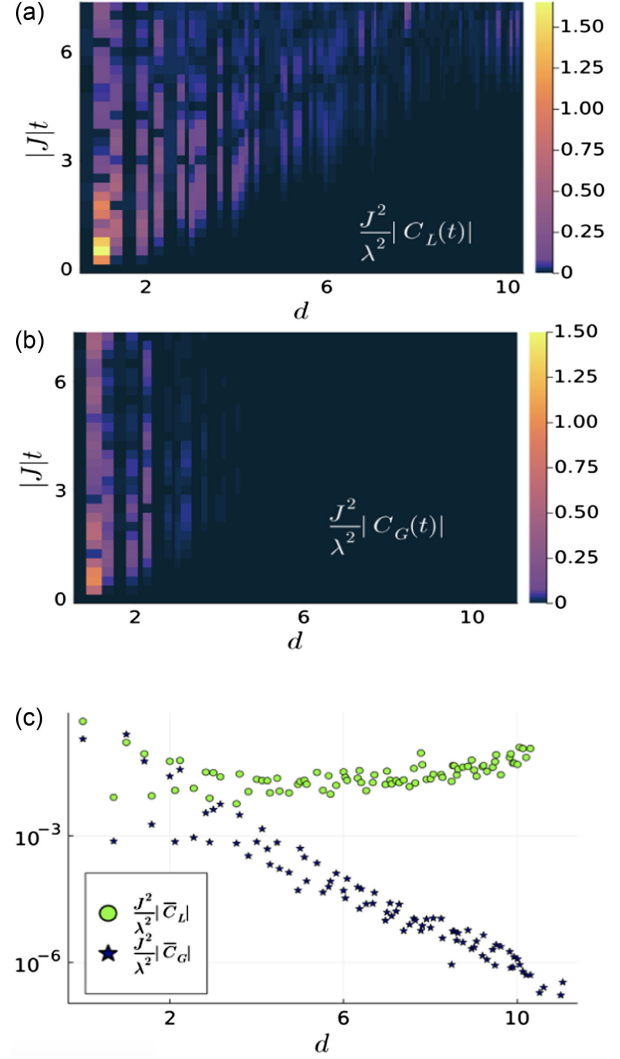


FIG. 2. Local and global information spreading quantified by $J^2/\lambda^2 |C_{L/G}(t)|$ for $|\lambda/J| = 0.2$. (a) Information spreading within an 18 plaquette cluster. (b) Information freezing in the full system. (c) Long time average vs distance for (a) and (b).

with a light conelike structure for information spread within a cluster, affirming the ergodic nature of large finite size clusters in this regime [8]. We choose $P = 18$ in this Letter, but similar results for C_L will hold for all large clusters. However, for the whole lattice, there is an exponential decay with a correlation length of around three to four lattice spacings, i.e., next-nearest-neighbor plaquettes, implying information freezing and saturation of entanglement growth. Such a qualitative difference is even more apparent in the long-time average of the commutators with distance in Fig. 2(c). Note that such information freezing is present for all values of $|\lambda/J|$ and is a generic feature of all disorder-free localized lattice gauge theories, where kinetic constraints induced by static charges, cause real-space fragmentation.

High temperature spectral functions.—We also calculate high-temperature ($T \gg \max(|\lambda|, |\mathbf{J}|)$) spectral functions,

which are relevant for neutron scattering experiments on frustrated magnets that might realize a U(1) QLM-type effective theory. To do so, one employs arguments from dynamical quantum typicality (DQT) [33,34] which state that a pure state drawn from a Haar-random distribution gives the same expectation values as the entire statistical ensemble. One can then define correlation functions as

$$\begin{aligned}
 S^{zz}(d, t, T) &= \frac{1}{N} \sum_{\mathbf{r}_i, \mathbf{r}_j \in \mathcal{L}} \frac{\langle \Phi_{\beta(t)} | \widehat{S}_{\mathbf{r}_i, \boldsymbol{\mu}}^z | \Phi_{\beta(t)} \rangle}{\langle \Phi_{\beta(0)} | \Phi_{\beta(0)} \rangle} + \epsilon \\
 &= \frac{1}{N'_d} \sum_{\substack{|\text{cl}| \\ <= P_c}} \sum_{\mathbf{r}_i, \mathbf{r}_j \in \text{cl}} \frac{\langle \Phi_{\beta_{\text{cl}}}(t) | \widehat{S}_{\mathbf{r}_i, \boldsymbol{\mu}}^z | \Phi_{\beta_{\text{cl}}}(t) \rangle}{\langle \Phi_{\beta_{\text{cl}}}(0) | \Phi_{\beta_{\text{cl}}}(0) \rangle} + \epsilon \quad (3)
 \end{aligned}$$

where $|\Phi_{\beta_{\text{cl}}}(t)\rangle = e^{-iH_{\text{cl}}t - \beta H_{\text{cl}}/2} |\psi_{\text{cl}}\rangle$, $|\varphi_{\beta_p}(t)\rangle = e^{-iH_{\text{cl}}t} \widehat{S}_{\mathbf{r}_j, \boldsymbol{\mu}}^z e^{-\beta H_{\text{cl}}/2} |\psi_{\text{cl}}\rangle$, $\beta = 1/T$, H_{cl} is the Hamiltonian in Eq. (1) but with the sum over all plaquettes belonging to cluster cl, and ϵ denotes the error which is exponentially small in the number of thermally occupied eigenstates. The typicality approach also works very well in a localized phase for large Hilbert spaces [35].

Taking the space-time Fourier transform of Eq. (3), gives the transverse component of the dynamical structure factor. As shown in Figs. 1 and 3(a), there are dominant delta-function-like peaks at low frequencies amidst a background of featureless response and a vanishing response as $\omega \rightarrow 0$. This is the hallmark of disorder-free localization and distinguishes it from paramagnetic response [9]. Such response remains robust on increasing system size and for all values of λ and J since the dominant peaks arise from the formation of small clusters (see next section) deep in the localized phase due to fragmentation induced by the static charges. The density of such clusters saturates at a constant value as a function of background charge density deep in the localized phase, smoothly decays across the localization transition, and then vanishes as a polynomial deep in the delocalized phase, as in standard percolation. Crucially, on crossing the localization transition, an infinite ergodic cluster emerges which has a continuous spectral response [8]. Hence, on crossing the transition from the localized side, there is a shift in weight from the discrete peaks to the continuous response.

However, the infinite cluster exhibits long-time hydrodynamic behavior with U(1) charge conservation. Assuming diffusion in 2D, i.e., a temporal decay of $t^{-d/2} = 1/t$, one would expect a logarithmic divergence of the spectral response as $\omega \rightarrow 0$. The localized phase, however, has no such contribution. Moreover, since the localization physics is dictated by the small clusters, there is a vanishing spectral response as $\omega \rightarrow 0$ due to their discrete and nondegenerate spectra.

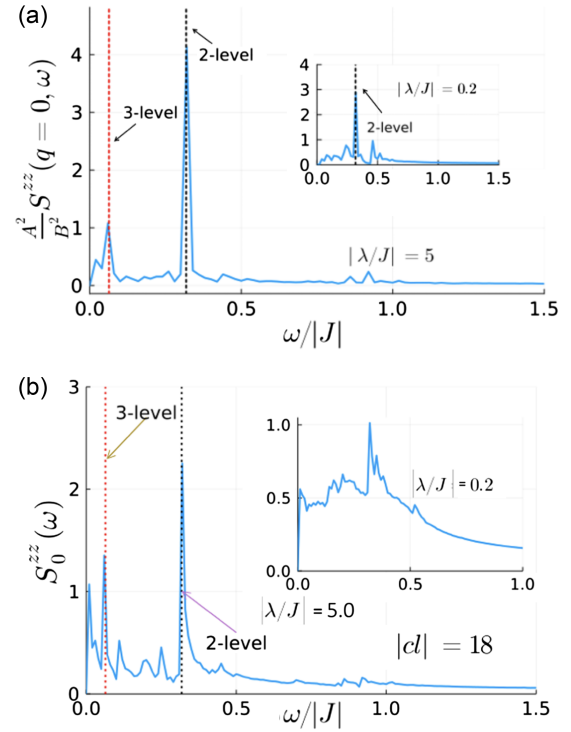


FIG. 3. Evidence of disorder-free localization from high temperature $[T = 5 \max(|\lambda|, |J|)]$ spatially averaged spectral functions. (a) The $q = 0$ component of the transverse component of the dynamic structure factor, $A = \max(|\lambda|, |J|)$ and $B = \min(|\lambda|, |J|)$, cutoff size $P_c = 18$ and $|\lambda/J| = 5.0$; (inset) same quantity as main plot, but for $|\lambda/J| = 0.2$. (b) On-site spectral function averaged over all spins belonging to all 18 plaquette clusters for $|\lambda/J| = 5.0$ and (inset) $|\lambda/J| = 0.2$.

Besides the above global signatures, local spectral functions like the temporal Fourier transform of onsite correlators, $S_0^{zz}(\omega)$, spatially averaged over spins belonging to all clusters of a particular size, evolve from a smooth curve with short bumps in the $|\lambda/J| \ll 1$ regime to a discrete set of peaks in the $|\lambda/J| \gg 1$ regime, as in Fig. 3(b). Such a difference indicates ergodic to nonergodic crossover within large but finite clusters [8].

Analytic estimate of dominant peaks.—The position of the peaks observed above can be accurately estimated from local physics of clusters of few plaquettes which form two and three level systems. Consider a two level system, for example a single flippable plaquette, the eigenvalues of such a system will be $-\lambda + J$ and $-\lambda - J$. Such a system should have a discrete peak at $\omega = J/\pi$. Similarly, for a two-plaquette system with three states (11/10/01; 1-flippable and 0-unflippable), the transition between the closest spaced pair is given by a discrete peak at $\omega = J^2/(\lambda\pi)$ in the $|\lambda/J| \gg 1$ regime. The dominance of these peaks arising from such local physics implies (i) on the global scale the dominant response deep in the localized phase is from the small clusters and (ii) in the $|\lambda/J| \gg 1$ regime, for the local spectral functions the physics of larger

clusters is effectively dominated by local motifs which form two- or three-level systems. Since within a cluster there is no real-space fragmentation, the local motifs arise purely due to interference effects. However, the nonergodic response in the local spectral functions averaged over connected clusters is a finite-size effect with dominant discrete peaks over a wide range of large finite-size clusters, which we call the disorder-free localization regime, similar to the many-body localization regime [36]. Their spectral weight eventually decreases on increasing size giving way to a continuous spectrum in the infinite-size limit [8]. However, the former contribution, due to fragmented clusters in typical sectors, remains discrete as the presence of a finite density of charges will always induce real-space fragmentation and form small clusters. These clusters have the same spectra irrespective of their position; hence even after spatial averaging a sharp response remains in all regimes of the Hamiltonian.

Discussion and outlook.—In this Letter we have presented numerical results for spatially averaged spectral functions in 2D as characteristic evidence for disorder-free localization. Local spectroscopic signatures have also been proposed for conventional disordered MBL, as a way to distinguish between strong and weak MBL [37,38]. However, most sharp spectral features are blurred out on spatial averaging, with a soft spectral gap at zero frequency being the only distinct consequence of both kinds of MBL. For the disorder-free localized phase, there are dominant sharp peaks in the dynamical structure factor as well as a vanishing response as $\omega \rightarrow 0$; both of these can, in principle, be observed in spectroscopic experiments. Our Letter can be translated to higher dimensions and could serve as evidence for quantum spin ice materials, where the analog of the charges would be orphan spins or dopants, and could be an alternate route to verifying the underlying gauge theory structure of such materials.

Simulating gauge theories in quantum simulators has been an area of current experimental effort, where mechanisms have been proposed to protect the gauge symmetry [39–43]. Our spectral features, which result in persistent oscillations of any gauge invariant observable at certain frequencies, provide a concrete probe to verify that the simulator does indeed realize a gauge theory. Moreover, our results on the unequal-time commutators further motivate lattice gauge theories as a fertile platform to probe information spreading and chaos. Further, lattice gauge theory with mobile matter adds a dynamic charge to the problem and is an interesting future direction.

The data for the figures are openly available on Zenodo at [44].

We thank Hongzheng Zhao and Adam McRoberts for valuable discussions. This project has received funding from the European Research Council (ERC) under the European Union’s Horizon 2020 research and innovation

programme (Grant Agreement No. 853443), and M. H. further acknowledges support by the Deutsche Forschungsgemeinschaft via the Gottfried Wilhelm Leibniz Prize program. This work was in part supported by the Deutsche Forschungsgemeinschaft under Grants No. SFB 1143 (project-id 247310070) and the cluster of excellence ct.qmat (EXC 2147, project-id 390858490).

*Corresponding author: nilotpal@pks.mpg.de

- [1] E. Fradkin, *Field Theories of Condensed Matter Physics* (Cambridge University Press, Cambridge, England, 2013).
- [2] R. Moessner and J. E. Moore, *Topological Phases of Matter* (Cambridge University Press, Cambridge, England, 2021).
- [3] R. Moessner and S. L. Sondhi, *Phys. Rev. B* **68**, 184512 (2003).
- [4] M. Hermele, M. P. A. Fisher, and L. Balents, *Phys. Rev. B* **69**, 064404 (2004).
- [5] A. Smith, J. Knolle, D. L. Kovrizhin, and R. Moessner, *Phys. Rev. Lett.* **118**, 266601 (2017).
- [6] M. Brenes, M. Dalmonte, M. Heyl, and A. Scardicchio, *Phys. Rev. Lett.* **120**, 030601 (2018).
- [7] P. Karpov, R. Verdel, Y.-P. Huang, M. Schmitt, and M. Heyl, *Phys. Rev. Lett.* **126**, 130401 (2021).
- [8] N. Chakraborty, M. Heyl, P. Karpov, and R. Moessner, *Phys. Rev. B* **106**, L060308 (2022).
- [9] P. H. Conlon and J. T. Chalker, *Phys. Rev. Lett.* **102**, 237206 (2009).
- [10] I. Papaefstathiou, A. Smith, and J. Knolle, *Phys. Rev. B* **102**, 165132 (2020).
- [11] W.-H. Li, X. Deng, and L. Santos, *Phys. Rev. Lett.* **127**, 260601 (2021).
- [12] G.-Y. Zhu and M. Heyl, *Phys. Rev. Res.* **3**, L032069 (2021).
- [13] T. Hodson, J. Willsher, and J. Knolle, *Phys. Rev. B* **104**, 045116 (2021).
- [14] J. C. Halimeh, H. Zhao, P. Hauke, and J. Knolle, *arXiv:2111.02427*.
- [15] S. Chandrasekharan and U.-J. Wiese, *Nucl. Phys.* **B492**, 455 (1997).
- [16] D. Horn, *Phys. Lett. B* **100**, 149 (1981).
- [17] P. Orland and D. Rohrlich, *Nucl. Phys.* **B338**, 647 (1990).
- [18] U.-J. Wiese, *Ann. Phys. (Berlin)* **525**, 777 (2013).
- [19] A. Y. Kitaev, *Ann. Phys. (Amsterdam)* **303**, 2 (2003).
- [20] D. S. Rokhsar and S. A. Kivelson, *Phys. Rev. Lett.* **61**, 2376 (1988).
- [21] R. Moessner and S. L. Sondhi, *Phys. Rev. B* **63**, 224401 (2001).
- [22] N. Shannon, G. Misguich, and K. Penc, *Phys. Rev. B* **69**, 220403(R) (2004).
- [23] See Supplemental Material at <http://link.aps.org/supplemental/10.1103/PhysRevLett.131.220402> for details of the percolation model and disorder-free localization in general, which includes Refs. [24–26].
- [24] M. van Horssen, E. Levi, and J. P. Garrahan, *Phys. Rev. B* **92**, 100305(R) (2015).
- [25] M. Schulz, C. A. Hooley, R. Moessner, and F. Pollmann, *Phys. Rev. Lett.* **122**, 040606 (2019).
- [26] N. Y. Yao, C. R. Laumann, J. I. Cirac, M. D. Lukin, and J. E. Moore, *Phys. Rev. Lett.* **117**, 240601 (2016).

- [27] J. C. Halimeh, P. Hauke, J. Knolle, and F. Grusdt, [arXiv: 2206.11273](#).
- [28] A. Metavitsiadis, A. Pidotella, and W. Brenig, *Phys. Rev. B* **96**, 205121 (2017).
- [29] J. Maldacena, S. H. Shenker, and D. Stanford, *J. High Energy Phys.* **08** (2016) 106.
- [30] P. Sala, T. Rakovszky, R. Verresen, M. Knap, and F. Pollmann, *Phys. Rev. X* **10**, 011047 (2020).
- [31] V. Khemani, M. Hermele, and R. Nandkishore, *Phys. Rev. B* **101**, 174204 (2020).
- [32] C. W. von Keyserlingk, T. Rakovszky, F. Pollmann, and S. L. Sondhi, *Phys. Rev. X* **8**, 021013 (2018).
- [33] R. Steinigeweg, J. Gemmer, and W. Brenig, *Phys. Rev. Lett.* **112**, 120601 (2014).
- [34] T. A. Elsayed and B. V. Fine, *Phys. Rev. Lett.* **110**, 070404 (2013).
- [35] R. Steinigeweg, J. Herbrych, F. Pollmann, and W. Brenig, *Phys. Rev. B* **94**, 180401(R) (2016).
- [36] A. Morningstar, L. Colmenarez, V. Khemani, D. J. Luitz, and D. A. Huse, *Phys. Rev. B* **105**, 174205 (2022).
- [37] R. Nandkishore, S. Gopalakrishnan, and D. A. Huse, *Phys. Rev. B* **90**, 064203 (2014).
- [38] S. Johri, R. Nandkishore, and R. N. Bhatt, *Phys. Rev. Lett.* **114**, 117401 (2015).
- [39] C. Schweizer, F. Grusdt, M. Berngruber, L. Barbiero, E. Demler, N. Goldman, I. Bloch, and M. Aidelsburger, *Nat. Phys.* **15**, 1168 (2019).
- [40] Z.-Y. Zhou, G.-X. Su, J. C. Halimeh, R. Ott, H. Sun, P. Hauke, B. Yang, Z.-S. Yuan, J. Berges, and J.-W. Pan, *Science* **377**, 311 (2022).
- [41] J. C. Halimeh, L. Homeier, H. Zhao, A. Bohrdt, F. Grusdt, P. Hauke, and J. Knolle, *PRX Quantum* **3**, 020345 (2022).
- [42] G. Semeghini, H. Levine, A. Keesling, S. Ebadi, T. T. Wang, D. Bluvstein, R. Verresen, H. Pichler, M. Kalinowski, R. Samajdar *et al.*, *Science* **374**, 1242 (2021).
- [43] B. Yang, H. Sun, R. Ott, H.-Y. Wang, T. V. Zache, J. C. Halimeh, Z.-S. Yuan, P. Hauke, and J.-W. Pan, *Nature (London)* **587**, 392 (2020).
- [44] N. Chakraborty, M. Heyl, P. Karpov, and R. Moessner, Zenodo, [10.5281/zenodo.7529643](#) (2023).